Acta Biomaterialia 7 (2011) 3196–3208

Contents lists available at ScienceDirect

Acta Biomaterialia

journal homepage: www.elsevier.com/locate/actabiomat

Biodegradable CaMgZn bulk metallic glass for potential skeletal application

Y.B. Wang [a,b,1], X.H. Xie [c,1], H.F. Li [a,b], X.L. Wang [c], M.Z. Zhao [b], E.W. Zhang [a,b], Y.J. Bai [b], Y.F. Zheng [a,b,*], L. Qin [c,d,*]

[a] State Key Laboratory for Turbulence and Complex Systems and Department of Advanced Materials and Nanotechnology, College of Engineering, Peking University, Beijing 100871, People's Republic of China
[b] Center for Biomedical Materials and Tissue Engineering, Academy for Advanced Interdisciplinary Studies, Peking University, Beijing 100871, People's Republic of China
[c] Department of Orthopaedics and Traumatology, The Chinese University of Hong Kong, Hong Kong SAR, People's Republic of China
[d] Translational Medicine Research and Development Center, Institute of Biomedical and Health Engineering, Shenzhen Institute of Advanced Technology, The Chinese Academy of Sciences, Shenzhen, People's Republic of China

ARTICLE INFO

Article history:
Received 9 December 2010
Received in revised form 27 April 2011
Accepted 27 April 2011
Available online 1 May 2011

Keywords:
CaMgZn
Bulk metallic glass
In vitro
In vivo
Biodegradable metal

ABSTRACT

A low density and high strength alloy, Ca65Mg15Zn20 bulk metallic glass (CaMgZn BMG), was evaluated by both in vitro tests on ion release and cytotoxicity and in vivo implantation, aimed at exploring the feasibility of this new biodegradable metallic material for potential skeletal applications. MTT assay results showed that the experimental CaMgZn BMG extracts had no detectable cytotoxic effects on L929, VSMC and ECV304 cells over a wide range of concentrations (0–50%), whereas for MG63 cells concentrations in the range ~5–20% promoted cell viability. Meanwhile, alkaline phosphatase (ALP) activity results showed that CaMgZn BMG extracts increased alkaline phosphatase (ALP) production by MG63 cells. However, Annexin V–fluorescein isothiocyanate and propidium iodide staining indicated that higher concentrations (50%) might induce cell apoptosis. The fluorescence observation of F-actin and nuclei in MG63 cells showed that cells incubated with lower concentrations (0–50%) displayed no significant change in morphology compared with a negative control. Tumor necrosis factor-α expression by Raw264.7 cells in the presence of CaMgZn BMG extract was significantly lower than that of the positive and negative controls. Animal tests proved that there was no obvious inflammation reaction at the implantation site and CaMgZn BMG implants did not result in animal death. The cortical thickness around the CaMgZn BMG implant increased gradually from 1 to 4 weeks, as measured by in vivo micro-computer tomography.

1. Introduction

In the biomedical field metals, ceramics and polymers are used as biomaterials to perform certain functions or to act as functional replacements after organ or tissue damage or degeneration, such as in bone fracture fixation or bone defect repair. The strength and toughness required in load-bearing parts of the body make biomedical materials such as titanium alloys and stainless steel indispensable, although their ability to bond with human bone needs to be further improved.

Bioactive glasses and ceramics used clinically as bone substitutes, like hydroxyapatite (HA), Bioglass®, and apatite–wollastonite (A–W) glass ceramics, offer biocompatibility as they contain ions commonly found in the physiological environment (Ca^{2+}, K^{+}, Na^{+}, Mg^{2+}, etc.) [1–4], and induce specific biological responses at the interface between the material and tissues [5]. However, they lack mechanical strength and are limited to use as fillers for bony defects and cannot be totally dissolved [6]. The development of biodegradable implant materials has attracted both academic and commercial attention in an attempt create the ideal feature, that it can eventually be absorbed by the human body. However, the currently available biodegradable implants are far from perfect for orthopedic applications [7].

Exploratory studies of bulk metallic glasses (BMGs) for biomedical applications have attracted significant attention recently [8,9]. In the light of their combination of greater mechanical strength, hardness and greater corrosion resistance several alloy systems, such as Ti-based, Zr-based, and Fe-based BMGs, have been developed with the purpose of using BMGs as load-bearing components [10–20]. As a pioneering work Zberg [21,22] carried out in vivo studies on MgZnCa BMG biomaterials and found them to be biocompatible, and that hydrogen production was significantly

* Corresponding authors. Address: State Key Laboratory for Turbulence and Complex Systems and Department of Advanced Materials and Nanotechnology, College of Engineering, Peking University, Beijing 100871, People's Republic of China. Tel./fax: +86 10 6276 7411 (Y.F. Zheng), Department of Orthopaedics and Traumatology, The Chinese University of Hong Kong, Hong Kong (L. Qin).
E-mail addresses: yfzheng@pku.edu.cn (Y.F. Zheng), lingqin@cuhk.edu.hk (L. Qin).
[1] These authors are joint first authors.

1742-7061/$ - see front matter © 2011 Acta Materialia Inc. Published by Elsevier Ltd. All rights reserved.
doi:10.1016/j.actbio.2011.04.027

reduced by the zinc- and oxygen-rich passivating layer. Our recent in vitro work on MgZnCa BMG has also proved their excellent in vitro biocompatibility [23]. The potential for use as bio-implants is due to, on the one hand, the biocompatible elements and, on the other, the required mechanical strength [24]. However, the glass forming ability of Mg–Zn–Ca ternary BMG are limited, with a largest critical size diameter (D_c) of only up to 5 mm reported in the literature to date [25].

Meanwhile, we note that Ca-based BMG have the same biomedical potential as Mg-based ones, especially Ca–Mg–Zn ternary systems. They have the same superior properties for use as biomaterials as Mg–Zn–Ca systems in many ways, and much better glass forming ability. The D_c value reported by Park is as high as 15 mm and it can be cast using a conventional copper mold under air [26,27]. The biomedical application potential has also been pointed out by some researchers [28,29]. However, the biocorrosion properties and biocompatibility have not yet been investigated and whether or not it is suitable to be used as a biomaterial remains unknown.

From the viewpoint of the authors of the present study low density Ca-based BMG might open up a new path for biodegradable implants, because of their combination of mechanical strength and glass bioactivity, like Ca-based bioceramics, and Ca-based BMG also has a low modulus close to that of natural bone [28,30]. Among all the Ca-based BMGs developed since the first report in 2002 [31,32] the Ca65Mg15Zn20 ternary BMG system has the greatest potential for medical application, because of two major characteristics: satisfactory mechanical properties [30] and a high glass forming ability [26]. In addition, its biocompatible constituents, i.e. calcium, magnesium and zinc, make itself an exciting candidate for human applications: (1) Ca is probably the most studied nutrient in bone health as the adult human body contains about 1000–1500 g Ca [33]; (2) Mg is necessary for calcium incorporation into bone, and so the co-release of Mg and Ca ions might be expected to be beneficial for bone healing [33–35]; (3) Zn has been reported to stimulate bone fracture healing, reduce postmenopausal bone loss, improve bone mineralization and skeletal strength [36–39]. Our interest in studying this CaMgZn BMG is the hope of obtaining biodegradable materials composed of essential human elements with improved mechanical properties. In order to fully understand the biocompatibility and biodegradability before any further consideration of using it as a biomaterial in vitro tests were carried out, the MTT assay, observation of the cytoskeleton organization, apoptosis detection and ALP determination to access cytotoxic effects, followed by in vivo tests involving implantation, X-ray observation and micro-computer tomography (micro-CT) reconstruction.

2. Materials and methods

2.1. Materials and characterization

Ca65Mg15Zn20 (nominal composition in at.%, hereafter termed CaMgZn) BMG samples were fabricated by copper mold injection casting under an argon atmosphere. In brief, high purity elements (99.5% Ca, 99.99% Mg and 99.99% Zn) were placed in a quartz tube and induction melted, then the melt were quickly injected into a copper mold and finally rod samples were obtained. X-ray diffraction (XRD) was performed to verify the amorphous structure of the samples using Cu K_α radiation at a scan rate of 4° min^{-1} (Rigaku-D/maxrB diffractometer operated at 40 kV and 100 mA at room temperature). Differential scanning calorimetry (Q100, Thermal Analysis Corp.) was used to identify the thermal dynamic properties of prepared samples. The compression test was carried out at a strain rate of 1×10^{-4} using an Instron 3365 universal test machine.

2.2. Immersion test

The immersion test in Hank's solution was carried out according to ASTM-G31-72. Experimental samples ($5 \times 5 \times 2$ mm) were immersed in 25 ml solutions and the temperature was kept at 37 °C in a water bath. After degradation the corrosion products were centrifugated from the electrolytes and dried in air after dehydration in a graded series of alcohol. XRD was used to identify the phase composition and environmental scanning electron microscopy (ESEM) observation (AMRAY 1-1910 FE, 15 keV, 8 mm WD) was performed to identify the elemental composition and morphology [35].

2.3. Cell culture

Murine L-929 fibroblast cells, human ECV304 umbilical vein endothelial cells, rodent VSMC vascular smooth muscle cells, and osteoblast-like cell line MG63 were used, since they are routinely used for cytotoxicity evaluation and are relevant to the in vivo implantation site. L-929, ECV304, VSMC, and mouse macrophage cell line RAW264.7 were cultured in the Dulbecco's modified Eagle's medium (DMEM), with 10% fetal calf serum at 37 °C in a humidified atmosphere of 5% CO_2. MG63 were cultured in minimal essential medium (MEM) supplemented with 10% fetal calf serum and 100 U ml^{-1} penicillin and 100 μg ml^{-1} streptomycin at 37 °C in a humidified atmosphere of 5% CO_2 [23].

2.4. Preparation of extracts

CaMgZn BMG samples were extracted in serum-free DMEM or MEM (Gibco-BRL, Paisley, UK) according to ISO 10993/12, i.e. 1 g material per 5 ml extraction liquid and incubation at 37 °C for 72 h. The negative control, an appropriate amount of DMEM/MEM, was poured into a polystyrene flask for cell culture and treated as the material extracts. After incubation the extracts were centrifuged and added to 10% fetal bovine serum, 100 U ml^{-1} penicillin and 100 μg ml^{-1} streptomycin.

2.5. MTT assay

Indirect cytotoxicity tests were carried out according to the standard procedure ISO 10993-5:1999, using L929, VSMC, ECV304 and MG63 cells and the MTT assay. 5×10^3 cells per 100 μl of medium were placed in each well of a 96-well cell culture plate and incubated for 24 h for cell attachment. The medium was then replaced with 100 μl of extract at concentration gradients of 100%, 80%, 60%, 50%, 40%, 30%, 20%, 15%, 10% and 5%. After 1, 2 and 4 days incubation 10 μl of MTT was added to each well and incubated for 4 h. Then 100 μl of formazan solubilization solution was added to each well. Twelve-hour later spectrophotometric measurements were carried out at 570 nm using an Elx-800 (Bio-Tek Instruments), with a reference at 630 nm.

2.6. Cytoskeleton organization

After 4 days culture with CaMgZn BMG extract the MG63 cell were prepared for cytoskeleton examination by fluorescence microscopy (Olympus IX71). Samples were rinsed three times with phosphate-buffered saline (PBS) and then fixed with 4% paraformaldehyde for 30 min at room temperature, and washed again with PBS. The fixed cells were permeabilized in 0.1% Triton X-100 (Sigma) for 5 min and washed three times in PBS. The cells were incubated with 5 μg ml^{-1} rhodamine–phalloidin (Sigma) for 30 min at 4 °C. After three washes with PBS the cells were stained with 10 μg ml^{-1} 4,6-diamino-2-phenyl-indole (DAPI) (Sigma) for 15 min. The samples were mounted under coverslips using

Vectashield medium and were then visualized using fluorescence microscopy.

2.7. Annexin V–fluorescein isothiocyanate (FITC) apoptosis detection

Apoptosis was measured using the annexin V–FITC apoptosis detection kit from Keygentec (Nanjing, China). This method detects externalization of phospholipids, which are normally located on the cytoplasmic surface of the cell membrane, via binding with the modified anticoagulant Annexin V. MG63 cells were plated at 60,000 per ml in 24-well plates and cultured for 4 days. Both adherent and floating cells were collected and resuspended in 1× cold binding buffer (10 mM HEPES, pH 7.4, 150 mM NaCl, 2.5 mM $CaCl_2$, 1 mM $MgCl_2$, 4% bovine serum albumin) for analysis. Cells were also stained with propidium iodide (PI) to detect dead cells. Analysis was in a FACSCalibur flow cytometer (Becton Dickinson) using CellQuest software (Becton Dickinson). Ten thousand cells were subjected to FACS analysis. Unstained cells were classified as "live", cells stained for annexin V only (early apoptotic) and cells stained for both annexin V and PI (late apoptotic) were combined and called "apoptotic", and cells stained for PI only were "dead".

2.8. Determination of ALP activity

Cellular ALP activity was determined by hydrolysis of p-nitrophenyl phosphate (p-Npp) using MG63 cells. Briefly, 100 μl of p-Npp dissolved at 1 mg ml^{-1} in buffer consisting of 0.1 M diethanolamine, 1 mM $MgCl_2$, and 0.5% Triton X-100, pH 10.5, was added to the cell pellets. After 30 min incubation at 37 °C the reaction was stopped by the addition of 50 μl of 0.3 M NaOH. The results are expressed as nmol p-nitrophenol (PNP) produced per min per well.

2.9. Sodium dodecyl phosphate–polyacrylamide gel electrophoresis (SDS–PAGE) and Western blotting

In order to ascertain osteopontin and collagen I expression after 4 days culture MG63 cells were analyzed using SDS–PAGE and Western blotting.

2.10. Quantification of cytokines by enzyme-linked immunoassay (ELISA)

To study the induction of proinflammatory mediators TNF-α production was analyzed by ELISA. After 18 h culture with extracts TNF-α determination in RAW264.7 cell culture supernatants was performed using commercially available ELISA kits (RapidBio Lab, Calabasas, CA) according to the manufacturer's instructions. The sensitivity was 10 pg ml^{-1}. Briefly, cells were incubated in 6-well plates at a density of 10^6 cells ml^{-1}. When the cells had grown to cover 80% of the plate area 15%, 30% or 50% CaMgZn BMG extract and fresh DMEM were added and cultured for 18 h. Each group had had sub-wells, and the experiments were repeated three times.

2.11. Animal tests

Three-month-old C57BL/6 mice were used to investigate the in vivo degradation properties of CaMgZn BMG and host bone responses. In brief, the mice were anesthetized via intraperitoneal injection with a combination of ketamine (75 mg kg^{-1}) and xylazine (10 mg kg^{-1}). The left knee of the mice was exposed and a tunnel 0.7 mm in diameter and 5 mm in length was created in the medullary cavity from the distal femur along the axis of the femoral shaft. The sterilized CaMgZn BMG rod 0.7 mm in diameter and 5 mm in length was implanted into the bone tunnel. The wounds were then carefully sutured and the mice were housed in an environmentally controlled animal care laboratory after surgery. The animal experimental protocol was approved by the Animal Ethics Committee of the Chinese University of Hong Kong (10-126, DH/HA&P/8/2/1, Pt.11). The in vivo analyses included the following. (1) Sequential radiographs of the distal femur taken every week post-operation (30 kV, 3 s) for general inspection under general anesthesia. (2) In vivo micro-CT (viva CT40, Scanco Medical AG, Brüttisellen, Switzerland) at a voxel size of 20 μm, used to monitor the distal femur of mice at weeks 1, 2, 3 and 4 post-operation. The change in the CaMgZn BMG implant in the bone tunnel was measured using our published protocol [40]. The two-dimensional (2-D) images were acquired directly from the scanning and the three-dimensional (3-D) structure was reconstructed using the volume of interest (VOI), where an optimized threshold is used to isolate the bone and material from the background. The density changes in CaMgZn BMG and the changes in cortical bone around the CaMgZn BMG were measured on the digitally extracted tissue. (3) Four weeks after implantation the femora with the CaMgZn BMG implants were harvested and prepared for fixation using 10% buffered formalin and then processed for embedding in methylmethacrylate resin. The resin blocks were cut using a diamond saw (SP1600, Leica AG, Solms, Germany) into 200 μm undecalcified sections, perpendicular to the long axis of the femoral shaft. The cross-sections were ground and polished to a thickness of about 50 μm. They were stained with van Gieson stain and then observed by light microscopy. (4) Representative samples after micro-CT scanning were used for in situ SEM evaluation to study the morphology of the corrosion products, similar to in vitro evaluation described above.

2.12. Statistical analysis

All data are expressed as the means ± SD of 3–6 replicates. Statistical procedures were performed with SPSS 16.0. Differences between groups were analyzed using one-way ANOVA, followed by Tukey's test. $P < 0.05$ was considered statistically significant.

3. Results

3.1. In vitro degradation behavior of CaMgZn BMG in Hank's solution

The XRD pattern and DSC curve of CaMgZn BMG are shown in Fig. 1, showing a main hump at a diffraction angle (2θ) of about 30° and no Bragg peak corresponding to any crystalline phase. The T_g, T_x and ΔT_x values obtained from the DSC curve were 369, 406 and 37 K, respectively, which indicates that the experimental

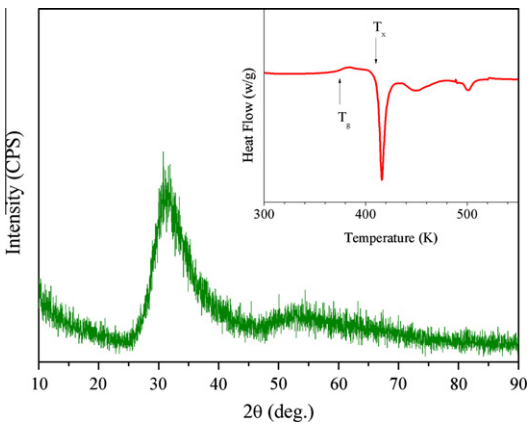

Fig. 1. XRD pattern and DSC curve of the experimental CaMgZn BMG.

CaMgZn BMG has a relatively high glass forming ability. The mechanical parameters obtained on compression testing of the CaMgZn BMG are 19.0 ± 1.3 GPa (Young's modulus), 354 ± 48 MPa (compression fracture strength) and 1.92 ± 0.15% (compression fracture strain), averaged from three samples for statistical comparison.

Composed of bioactive elements, it is expected that CaMgZn BMG might rapidly degrade in simulated body fluids. Thus we set out to characterize its degradation behavior by immersion tests. Fig. 2a shows hydrogen evolution volumes from the CaMgZn BMG in Hank's solution, with the inset showing the morphology of the corrosion products under SEM (after immersion in Hank's solution for 3 h), while Fig. 2b and c are the corresponding XRD and Fourier transform infrared (FTIR) spectroscopy results. The immersion test showed that plate-shaped CaMgZn BMG samples degraded rapidly and disintegrated completely after no more than 3 h in vitro. The energy-dispersive spectroscopy (EDS), XRD and FTIR spectroscopy results indicated that the corrosion products were mainly composed of calcium phosphate, calcium hydroxide, magnesium hydroxide, zinc hydroxide, calcium zinc hydroxide hydrate and other chemical compounds.

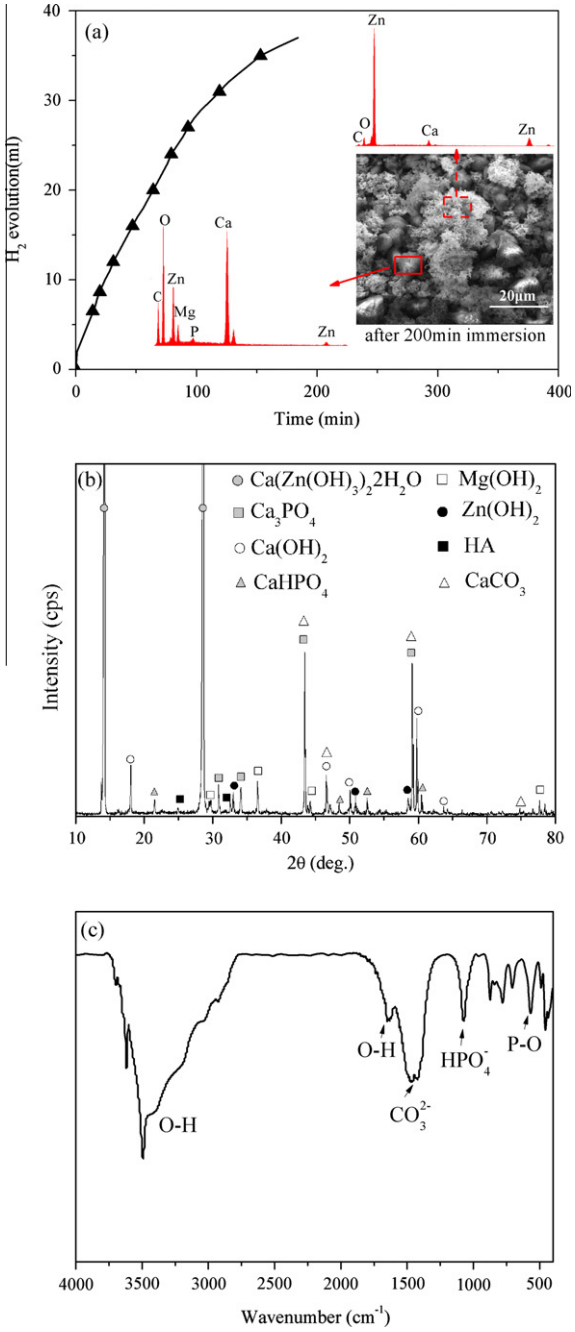

Fig. 2. Immersion of the CaMgZn BMG in Hank's solution. (a) Hydrogen evolution volume versus immersion time (the inset is a SEM image showing the morphology of the resulting corrosion products). (b) The corresponding XRD pattern of the corrosion products. (c) The corresponding FTIR curve of the corrosion products.

3.2. Cytotoxicity evaluation

Based on the degradation behavior, CaMgZn BMG sample extracts of graded concentration were used to evaluate the cytotoxicity to various cell lines. Fig. 3 illustrates the viability of MG63 cells after culture in CaMgZn BMG extracts of graded concentration expressed as a percentage of the viability of cells cultured in the negative control. The viability results for other cells (L929 cell, ECV304 cell and VSMC cell) are shown in Supplementary Figs. S1, S2 and S3. It was found that the viability was quite low for high concentration extracts for all the cell lines because of the pH change (pH >9 when the concentration was >50%). At concentrations lower than 30% the viabilities of four of the cell lines were higher than 75%, implying no cytotoxicity. Unlike other cells, MG63 cells had the highest cell viability at a concentration of 15% after culture for 1, 2 and 4 days. The 15% and 20% extracts had significantly higher values compared with the negative group ($P < 0.05$) after 4 days. The 40%, 50%, 60%, 80% and 100% extracts had significantly lower values compared with the negative group after culture for 4 days, while there was no significant difference for other concentrations.

3.3. Fluorescent labeling of F-actin and nuclei

Immunofluorescence staining was carried out to show cytoskeleton developments in MG63 cells after cultured with CaMgZn BMG extract. This cell line consistently and reproducibly exhibited a number of fundamental phenotypic characteristics of osteoblasts [41]. The distribution of actin filaments after treatment with CaMgZn BMG extract for 4 days was analyzed using rhodamine–phalloidin staining. As shown in Fig. 4, the control cells appeared as uniformly labeled cells with well-developed actin stress fibers (as shown in Fig. 4b). The shape of the cells treated with 15%

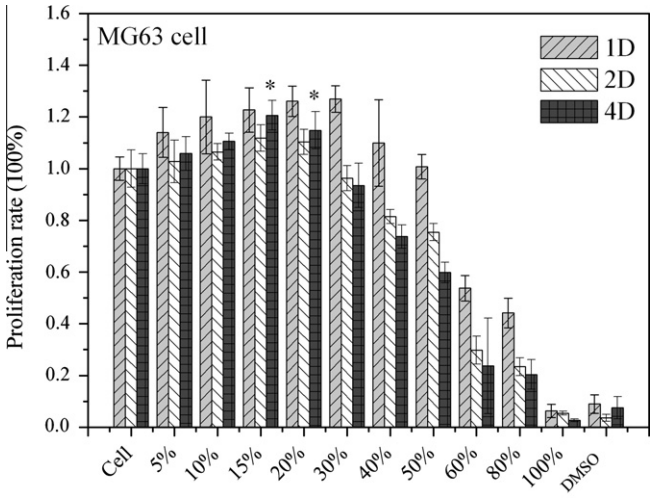

Fig. 3. Effect of CaMgZn BMG extracts on MG63 cell viability. *$P < 0.05$ compared with the negative control group.

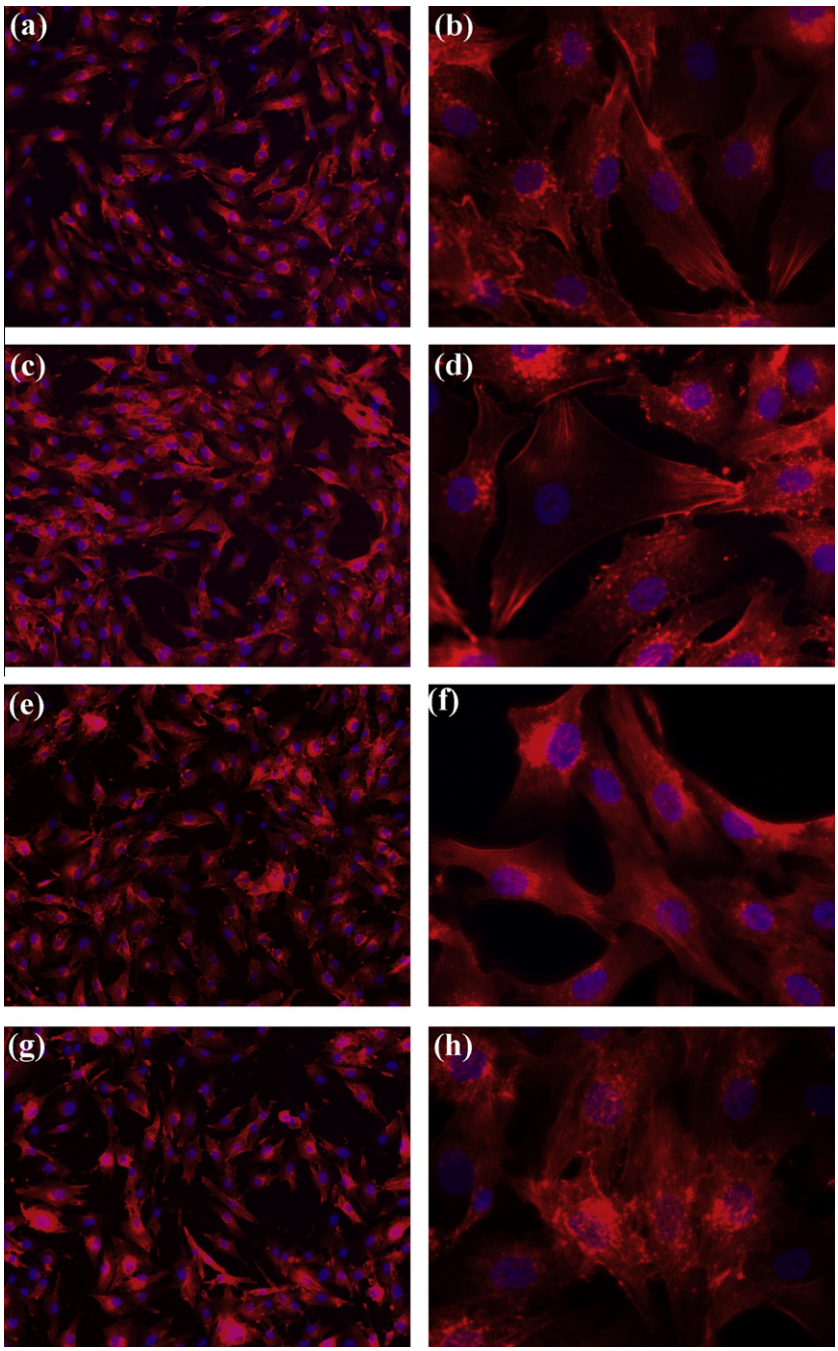

Fig. 4. MG63 cell morphology and fluorescence staining of F-actin and nuclei after incubation with CaMgZn BMG extracts for 4 days: (a and b) control cells; (c and d) 15% extracts; (e and f) 30% extracts; (g and h) 50% extracts.

extract exhibited no difference compared with control cells, with clear longitudinal stress fibers. After treatment with 30% extract the cells exhibited a spindle-like shape. The number of cells decreased significantly compared with the 15% extract group, but was close to the control group. In the 50% extract MG63 cells showed an irregular shape and the stress fibers were not as well stretched as in the other groups. The nuclei of cells in all groups can be clearly seen, with no distinguishable differences.

3.4. Apoptosis analysis

Quantitative evaluation of apoptosis was carried out by flow cytometry of MG63 cells stained with Annexin V–FITC and PI. This approach enabled a rough differentiation between cells undergoing apoptosis and necrosis. Cells that stained with annexin V–FITC but not with PI were regarded as early apoptotic, whereas those stained with PI only were regarded as necrotic. Staining with both probes indicated late apoptosis and/or secondary necrosis. According to this convention, as shown in Fig. 5 and Table 1, 50% CaMgZn BMG extract resulted in a greater degree of apoptotic cell death.

3.5. Effect of CaMgZn extract on ALP activity

In osteoblasts ALP expression is an early marker of osteogenic differentiation. Factors influencing ALP expression may further affect cell osteogenic mineralization ability. Fig. 6 reveals the ALP

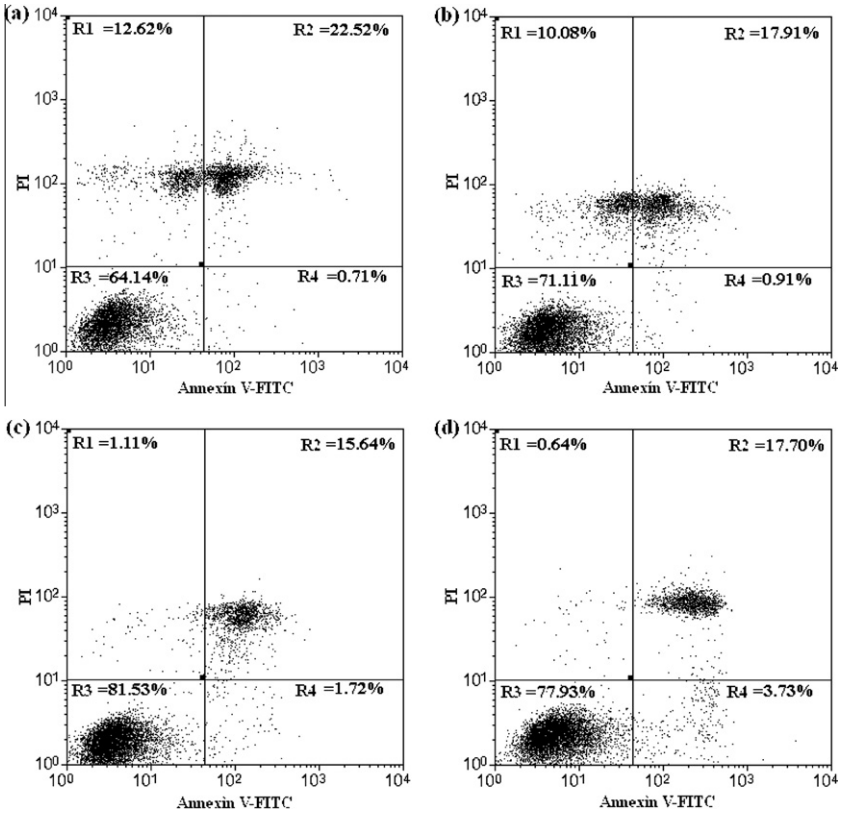

Fig. 5. Flow cytometric analysis of MG63 cells stained with Annexin V–FITC and PI after incubation (a) without, and with (b) 15% CaMgZn BMG, (c) 30% CaMgZn BMG, and (d) 50% CaMgZn BMG extract for 4 days. Control cells were incubated for the same time with MEM. Unchanged viable cells are located in R3, early apoptotic cells in R4 (Annexin V–FITC positive), non-viable or late apoptotic/necrotic cells in R2 (Annexin V–FITC/PI double positive) and non-viable necrotic cells/nuclear fragments in R1 (PI single positive).

Table 1
Apoptotic MG63 cell numbers after treatment with different concentrations of CaMgZn extract.

Groups	R1 (%)	R2 (%)	R3 (%)	R4 (%)
Negative control	12.62	22.52	64.14	0.71
15%	10.08	17.91	71.11	0.91
30%	1.11	15.64	81.53	1.72
50%	0.64	17.70	77.93	3.73

activity of MG63 cells after 4 days culture with CaMgZn BMG extract. It can be clearly seen that MG63 cells show greater ALP activity at a concentration of 15%, which is consistent with the above cell viability results. The 10%, 15% and 20% extracts had significantly higher values compared with the negative control group ($P < 0.05$). The 60%, 80% and 100% extracts (the 100% extract caused significant cell death, and the measured absorbance was <0) had significantly lower values compared with the negative control group, while there was no significant difference for other concentrations. It can be seen that, consistent with the MTT assay results, at concentrations of 10–20% CaMgZn BMG extracts have the ability to promote the growth of MG63 cells and further increase ALP production due to the greater cell numbers.

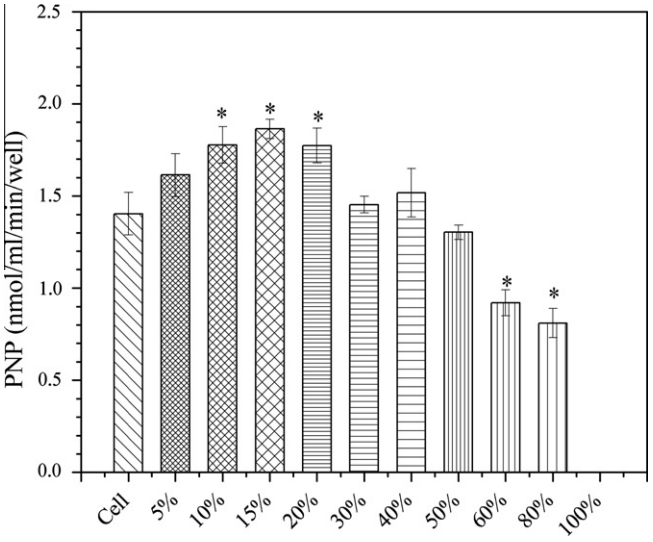

Fig. 6. ALP activity results for CaMgZn BMG extracts expressed as nmol ml^{-1} PNP produced per min per well. *$P < 0.05$ compared with negative group.

3.6. Western blotting

Fig. 7 shows the collagen I and osteopontin expression by MG63 cells after culture with CaMgZn BMG extracts for 4 days. Expression of the GAPDH housekeeping gene in cells exposed to all the culture media was homogeneous, while a slightly greater variability or no reduction in collagen I and osteopontin were observed when MG63 cells were exposed to 15% and 30% extracts compared with the negative control.

3.7. Effect of CaMgZn extract on TNF-α production

In order to investigate how CaMgZn BMG extracts modulate TNF-α synthesis, RAW264.7 cell were incubated with 15%, 30%

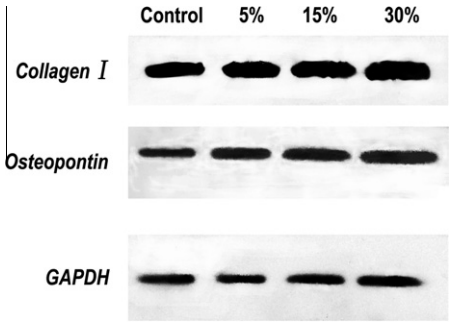

Fig. 7. Collagen I and osteopontin synthesis by MG63 cell cultured with CaMgZn BMG extracts determined by Western blotting.

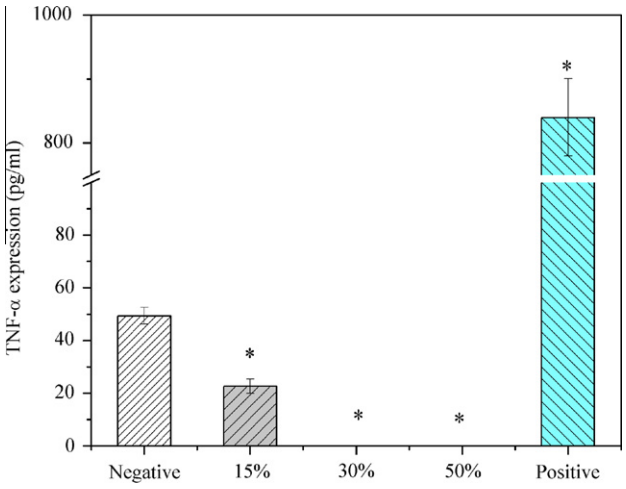

Fig. 8. Effect of CaMgZn BMG extracts on TNF-α mRNA expression by RAW264.7 cells. *$P < 0.05$ compared with negative group.

and 50% extracts for 18 h. As shown in Fig. 8, TNF-α mRNA production was higher when cells were exposed to the positive control. However, it is interesting to note that after 18 h cell exposure the production of TNF-α mRNA decreased, from the negative control to the 15%, 30% and 50% extracts. Higher concentrations of CaMgZn BMG extract do not stimulate higher production of TNF-α, which might be caused by a change in pH. Thus the degradation debris of TNF-α production should be considered further in future investigations.

3.8. Animal tests with CaMgZn bulk metallic glass rod implant

3.8.1. X-ray observation

There was no inflammation seen around the operation site and no mice died after surgery. Radiographs indicated that all the CaMgZn BMG rods were well positioned in the distal femur and no translucent areas were found (Fig. 9). With time after implantation the CaMgZn BMG rods lost their original integrity and were degraded and dispersed in the medullary cavity. After 1 week reactive hyperplasia of the bone was observed around the cortical zone of the distal femur. There was bone damage to the trabeculae of the distal femur, the metaphysis region that may induce further tissue–rod interaction, as well as further cellular responses. Clearly, different bone types respond differently to the CaMgZn rod.

3.8.2. Micro-CT observation

The results of micro-CT (Fig. 10) showed that the integrity of the CaMgZn BMG rods was maintained at 0 weeks and was clearly differentiable from the surrounding bony tissue, due to clear difference between the material and bone density (Fig. 10 B0, red represents high density, green low density and white intermediate density). There was an obvious gap between the CaMgZn BMG rods and the cortical bone from 2D images at 0 weeks (Fig. 10 A0). After 1 week the gap between the CaMgZn BMG rods and cortical bone was reduced and the debris from CaMgZn BMG rods was dispersed in the surrounding tissues. The density of the CaMgZn BMG rods decreased after 1 week compared with that at 0 weeks ($P < 0.05$). Although the average density of the CaMgZn BMG rods decreased gradually after 1, 2, 3 and 4 weeks, there were no statistical difference among the different time points, which may be explained by the rapid degradation and relatively slow absorption. There was no obvious difference in bone mineral density of the cortical bone around the implanted CaMgZn BMG rod (Fig. 11a). However, it was found that the thickness of the cortical bone around the CaMgZn BMG rods increased gradually from weeks 0 to 4. The bone formed around the cortical bone, which confirmed the results of the X-ray examination, indicated a strong periosteal stimulation by the CaMgZn BMG rods. The average thickness of cortical bone was 0.40 ± 0.17 mm at week 4, which was significantly higher than that at week 0 (0.25 ± 0.04 mm) (Fig. 11b, $P < 0.05$). The diameter of the bone marrow cavity around the CaMgZn BMG decreased from week 0 (1.51 ± 0.05 mm) to week 4 (2.12 ± 0.08 mm) (Fig. 11c, $P < 0.05$) and the bone shaft diameter, excluding periosteal expansion, increased slightly (Fig. 11d). This suggests that debris from the CaMgZn BMG rods may induce a stronger osteogenic effect in the periosteum, resulting in reactive bone hyperplasia during in vivo degradation. When the material was concomitantly degraded and dispersed the density of material close to the cortical bone was lower than that in the center of the material and was similar to that of cortical bone, so the interface between cortical bone and the edge of the material was not very clear because the 3-D image is based on density. The bone in the upper right region is newly formed bone, not degradation products of cortical bone, which may be observed in A1–A4. The bottom right region of A1–A4 (2-D) is the same as upper right area of B1–B4 (3-D). The disintegration of bone tissue in the upper right region is caused by the relatively low density of new bone, so some occurrences are not visible in the 3-D images but are clear in the 2-D images. They do not represent actual disintegration.

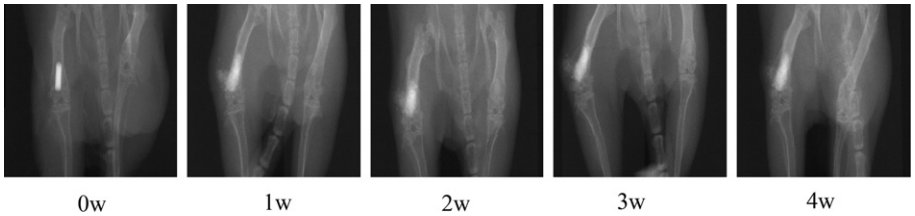

Fig. 9. Radiographs of mice with CaMgZn BMG rod implants at different times after surgery.

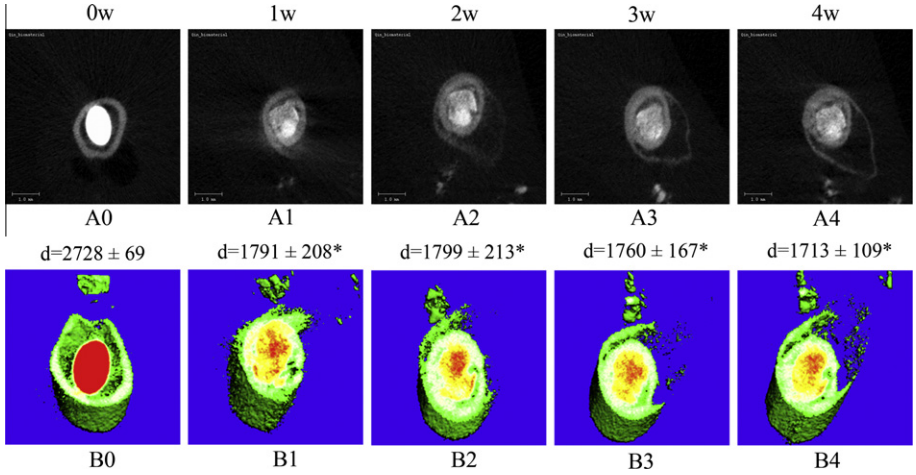

Fig. 10. Micro-CT images of distal femurs with CaMgZn BMG rod implants for different times after surgery. (A) 2D images; (B) 3D images. 0–4 refers to 0–4 weeks. '*d*' represents the density of the CaMgZn BMG rod (mg cm^{-3}). $^{*}P < 0.05$ compared with that at week 0 (baseline).

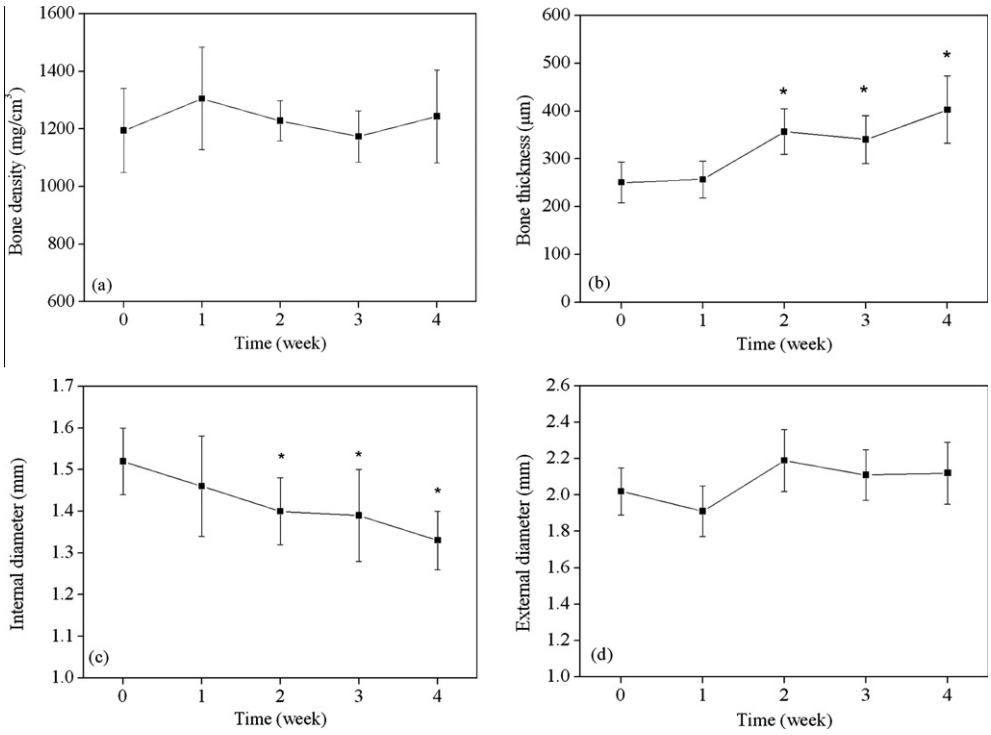

Fig. 11. Analysis of (a) the bone mineral density (BMD), (b) bone thickness, (c) bone marrow cavity diameter, and (d) bone shaft diameter. $^{*}P < 0.05$ compared with data for weeks 0 (baseline) and 1.

3.8.3. Histological analysis

The histological observations at 4 weeks after implantation showed that the bone thickness around the implanted CaMgZn BMG rod was higher than that of normal bone (Fig. 12), which was similar to the micro-CT results. The CaMgZn BMG rod had been degraded and the debris diffused into the bone marrow cavity, which might stimulate new bone formation at the inner edge of the residual cortical bone 4 weeks after implantation (Fig. 12b, arrows). When magnified (Fig. 12c) the new bone at the inner edge of the cortical bone was clearly observed (white arrows), with some particulate deposition of CaMgZn BMG (blue arrow). However, there was some osteolysis, and cartilage formation could be observed in the distal femur (Fig. 13), probably due to the rapid degradation and pH value increase.

3.8.4. SEM morphologies of corrosion products in situ

Fig. 14 shows cross-sectional SEM images of the corrosion products in the bone marrow cavity. The compositions of these particles were analyzed by EDS. As in the in vitro degradation test, the corrosion products were dispersed, in the form of small particles, which were also observed by micro-CT observation. These particles were mainly composed of Ca, Mg, Zn, C, O and P, indicating the formation of calcium phosphate and carbonate, as well as hydroxides, which is also consistent with the in vitro degradation results. The EDS results also show that the composition of the bone near the corrosion particles was not obviously changed compared with normal bone. Newly formed bone was also seen in the inner part of the bone, which is consistent with the micro-CT results.

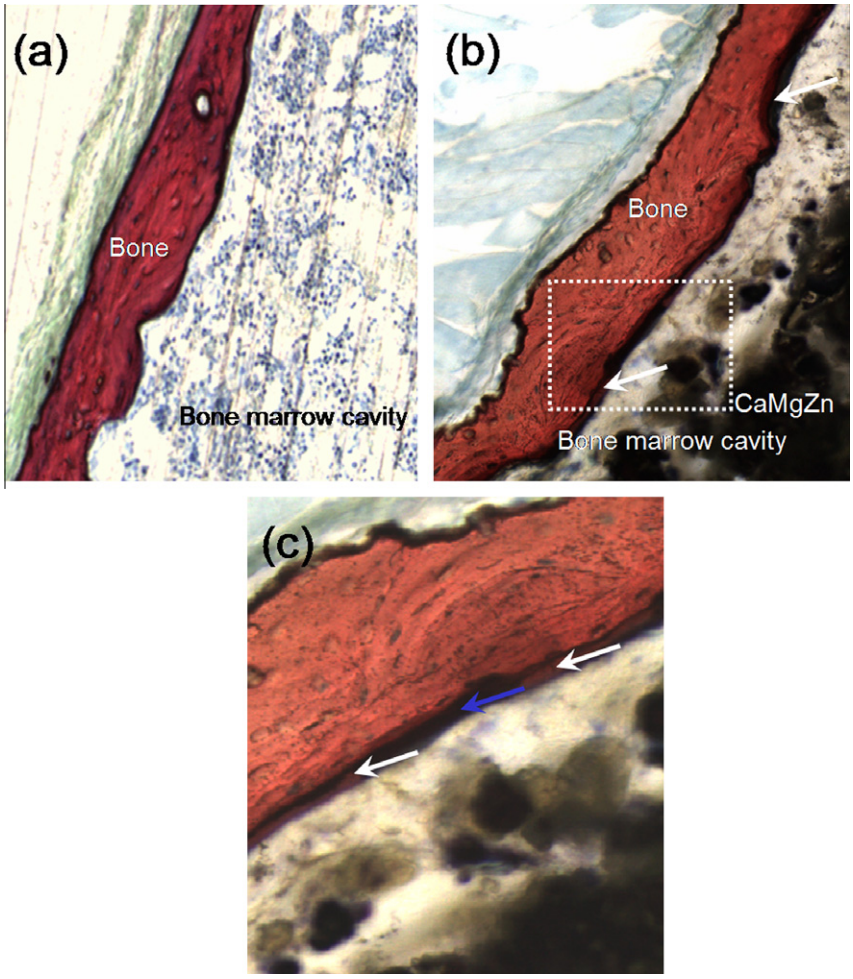

Fig. 12. Histological observation of cortical bone by light microscopy with Van Gieson staining. (a) Normal bone and the bone marrow cavity (5×); (b) CaMgZn BMG rod in the femur of a mouse 4 weeks after implantation, with new bone formed at the inner edge of the cortical wall (arrows) (5×); (c) magnification of the white rectangular frame (arrows indicate newly formed bone) (10×).

4. Discussion

The above results have shown that Ca65Mg15Zn20 BMG could degrade both in vitro and in vivo with good biocompatibility. It may fulfill the demand for high mechanical strength and biodegradable metallic materials with essential human elements. However, because of its rapid degradation rate both in vitro and vivo the following two aspects should be discussed for its future development.

4.1. Mechanism of biodegradation of CaMgZn BMG

CaMgZn alloys in the glassy state have been reported to be better oxidation resistant than in the crystalline state [30,42]. It would be hoped that it would have corrosion resistance. However, when placed in simulated body fluid in vitro an immediate reaction took place between the CaMgZn BMG and the culture medium. These chemical reactions become more complicated in the presence of various kin anions, which may accelerate dissolution of the CaMgZn BMG. Based on the results of the immersion test, XRD and FTIR spectroscopy analyses multiphase products were formed. The main corrosion reactions might happen as follows:

$$M + 2H_2O \rightarrow M(OH)_2 \downarrow + H_2 \uparrow (M = Ca, Mg, Zn) \quad (1)$$

$$Zn + 2OH^- \rightarrow ZnO \downarrow + H_2O \quad (2)$$

$$ZnO + Ca(OH)_2 + 3H_2O \rightarrow Ca[Zn(OH)_3]_2 \cdot H_2O \quad (3)$$

$$M^{2+} + PO_4^{3-} \rightarrow M_3(PO_4)_2 (M = Ca, Mg, Zn) \quad (4)$$

$$M^{2+} + CO_3^{2-} \rightarrow M_(CO_3)_2 (M = Ca, Mg, Zn) \quad (5)$$

Taking into consideration the above reactions, a biocorrosion model has been proposed, as illustrated in Fig. 15. (1) Hydroxides are first generated on the fresh surface of the CaMgZn BMG. The evolution of hydrogen makes the corrosion layer porous and non-protective. The surrounding solution continuously penetrates and reacts with the inner metal layer. (2) In the near surface zone a dissolution–precipitation mechanism occurs. Although $Ca(OH)_2$, $Mg(OH)_2$, and ZnO are thought to be indissoluble under normal conditions, in the presence of Cl^- and other anions the homeostasis of this process could be destroyed and corrosion of the CaMgZn BMG proceed. (3) During the process of biocorrosion apatite and carbonate are formed. Zberg reported that the formation of $ZnCO_3$ and ZnO could act as a protective layer in a Zn-rich, Mg-based BMG, accompanied by an increase in pH as the metal is dissolved into solution [21]. In our case Zn-rich products were formed on the surface of the CaMgZn BMG, (see Fig. 2a), but they did not stop the corrosion process. This might be related to reaction (3).

A much slower degradation process was evident in vivo than in vitro. After 4 weeks implantation some residual CaMgZn BMG remained, indicated by the red region (see Fig. 10 B4). Due to the confined area compared with the in vitro immersion tests this

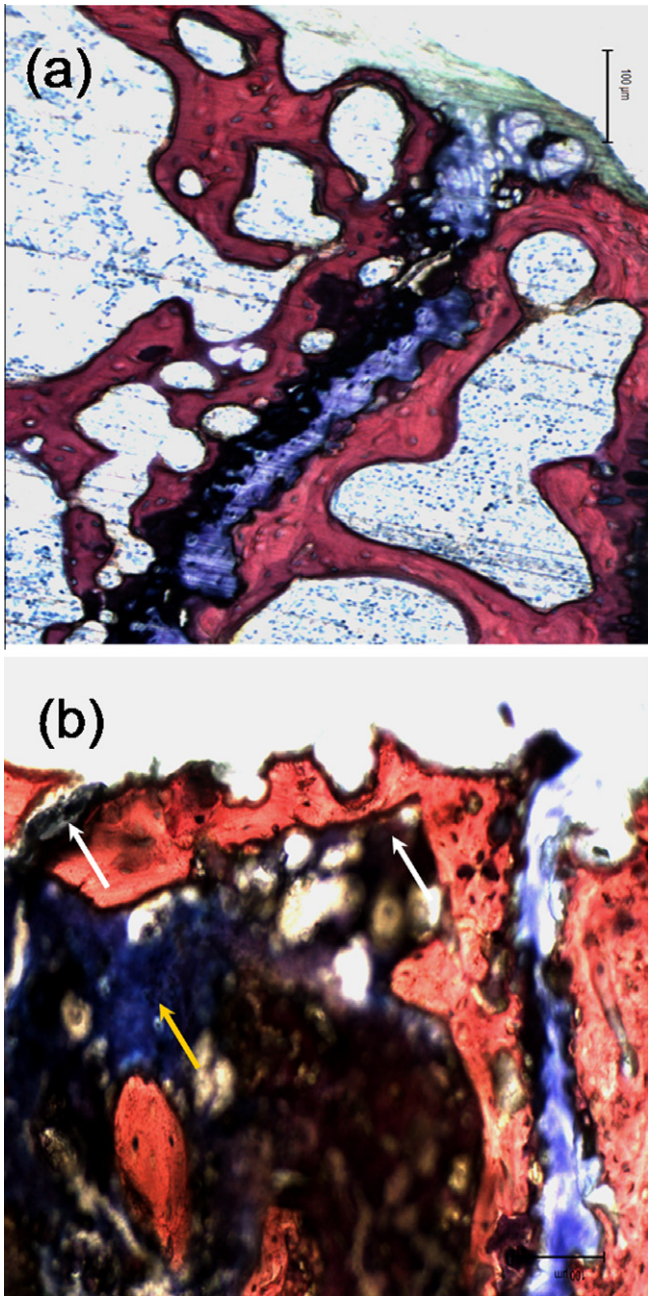

Fig. 13. Histological observation of distal femora by light microscopy with Van Gieson staining 4 weeks after implantation (5×). (a) Distal femur with normal trabecular bone and epiphysis; (b) CaMgZn BMG rod in the distal femur with osteolysis (white arrows) and newly formed cartilage (yellow arrow) in bone marrow cavity (5×). The bone marrow cavity was full with debris of degraded metallic glass.

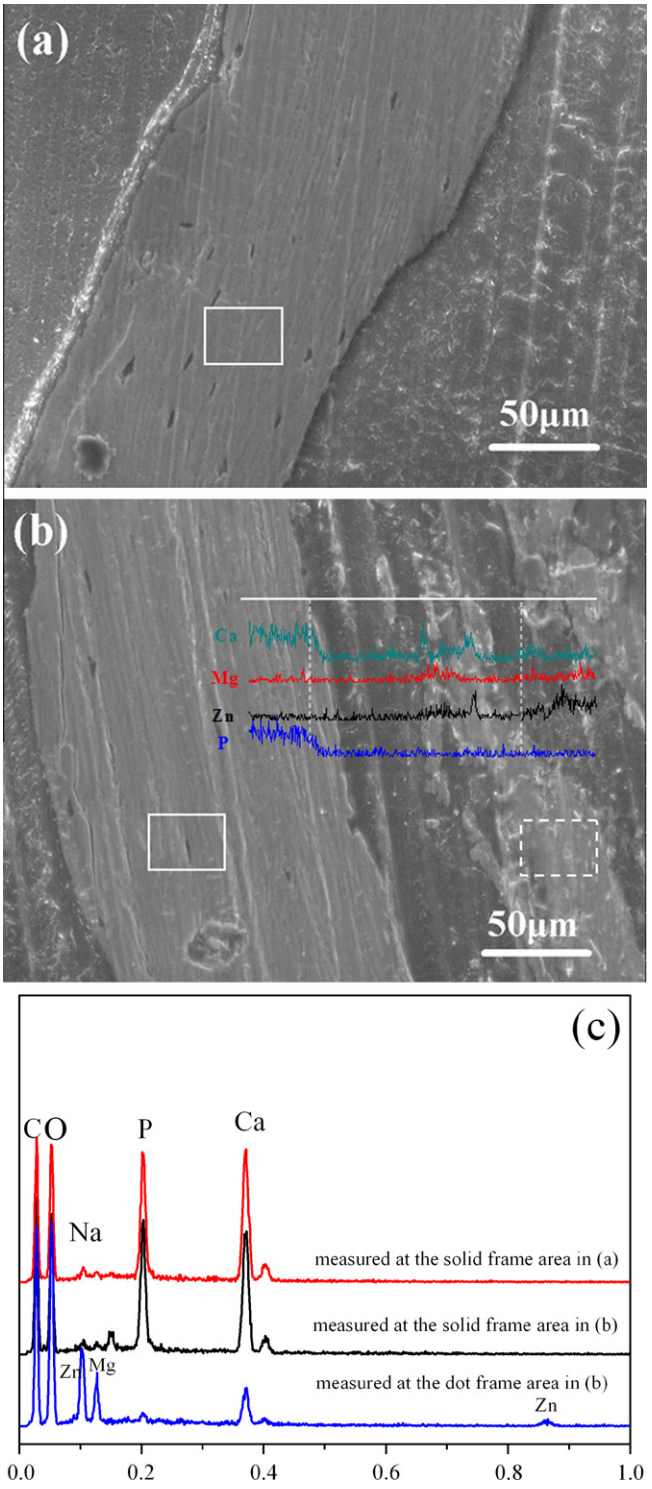

Fig. 14. SEM images of tissue slices and the corresponding EDS analysis. (a) Normal bone; (b) 4 weeks after implantation of a CaMgZn BMG rod, with the elemental distribution of the white line; (c) EDS of the white square region in (a) and white square region in (b).

can be put down to two causes. (1) 3-D micro-CT indicated that new bone was formed around the implants, which is consistent with other studies that calcium is an essential element in new bone mineralization [43,44]. In addition, in the presence of zinc and magnesium [34,38] the process of bone formation is accelerated, resulting in the much smaller marrow cavity found in the present study. At the same time volume expansion of the corrosion products filled the marrow cavity and slowed the penetration of body fluids deep into the alloy. (2) M^{2+} (M = Ca, Mg, or Zn) ions are supersaturated in the medullary space and numbers of phosphate ions are absorbed through electric charge attraction. The increased calcium phosphate formation means that anions are not as available near the interface as in the in vitro experiment. The supplementary of these anions from other part takes time, and may also slow down the corrosion process. Meanwhile, due to the relatively slow degradation rate it is suggested that the local pH was within the range of the surrounding tissues.

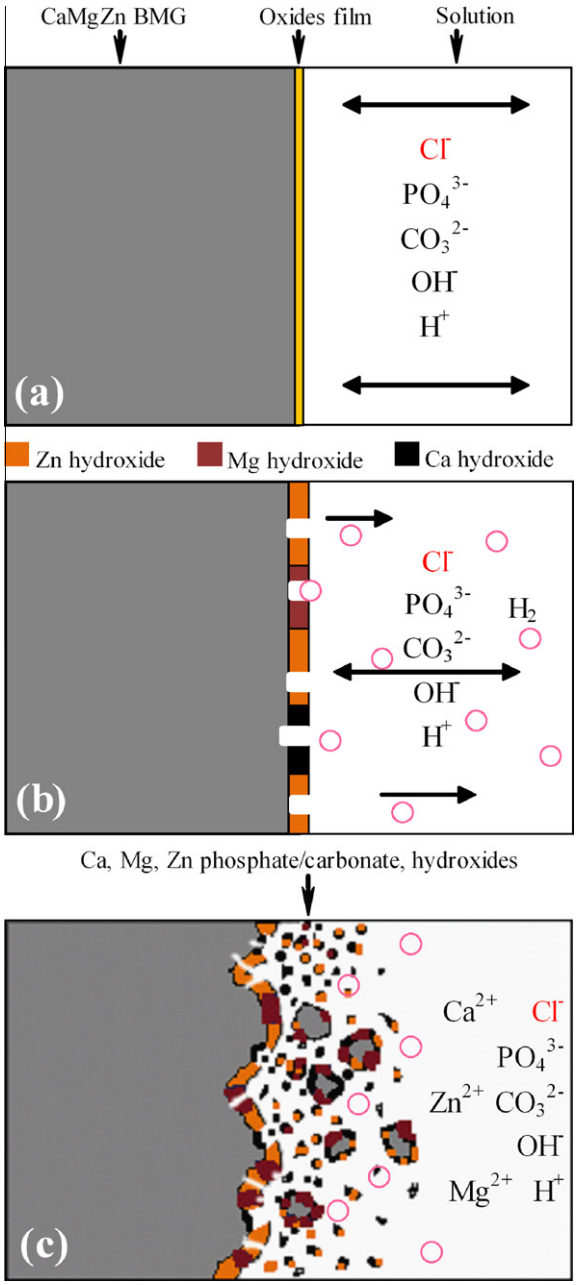

Fig. 15. Schematic corrosion of CaMgZn BMG in simulated body fluid.

4.2. Comparison of CaMgZn BMG with current Ca-based inorganic biomaterials

For the repair of bone in orthopedic surgery the ideal material should be biocompatible, biodegradable and osteoconductive in order to promote cell migration into the defect site and new bone formation [45]. The most widely used Ca-based inorganic biomaterials are HA, tricalcium phosphate (TCP) and bioglasses [46]. HA is one of the most biocompatible materials owing to its similarity to mineral constituents of teeth and bones. However, the mechanical properties of pure HA ceramics are poor, and they cannot be used as load-bearing implants, so its medical applications are limited to small unloaded implants, powders, coatings and low load porous implants [47,48]. TCP and bioglasses have the same weakness as HA [49], as listed in Table 2 [24,25,27,28,30,49–59]. From the point of view of the mechanical properties we understand that, although these bioceramics are extremely biocompatible, their use is still restricted by one or more aspects of their mechanical properties compared with human bone. When used in their dense forms both the Young's modulus and density of HA and TCP do not match human bone. As for bioglasses, the Young's modulus is still much higher than human bone. MgZnCa BMG have much closer values than the above three materials, but they still have higher Young's moduli. Apparently, CaMgZn BMG show the closest to ideal characteristics, with the closest Young's moduli to human bone, and adequate strength to accept a load. From the degradation point of view, the current Ca-containing bioceramics have either slow (like HA) or fast (like $CaSO_4$) degradation rates, which do not match the time for bone healing. CaMgZn BMG exhibit even faster degradation times than that of $CaSO_4$.

Except for their unsatisfactory mechanical properties, these bioceramics are biocompatible mainly because of their close compositional similarity to the inorganic constituents of human bone, e.g. HA. As for TCP, it degrades to HA [49]. Thus current bioceramics only show an osteoconductive ability rather than an osteoinductive ability. As for CaMgZn BMG, in the presence of enough Ca new bone could be inductively formed around the implant. Both in vitro and in vivo tests showed that CaMgZn BMG has the ability to promote bone formation through a mechanism of both endosteal and periosteal bone formation. So, unlike current bioceramics, which are only extrinsic substituents replacing damaged bone, the new bone formed in the presence of CaMgZn BMG is derived from endogenous reactions. This might be another advantage for its potential application in orthopedics.

However, one recognizable drawback of CaMgZn BMG is the relatively rapid degradation rate, which will result in a loss of mechanical strength of the BMG. It is better for the BMG to degrade and lose its mechanical strength slowly, in combination with increased bone formation around material. So surface modification techniques are necessary in order to slow down the degradation rate in order to maintain the mechanical support functions over a longer period. In our early work several biocompatible films were deposited on the CaMgZn surface and showed favorable effects [60]. Based on biomaterials currently in use in clinical applications we think that the following coatings may be beneficial in the use of CaMgZn BMG as biomaterials: Si coatings, HA coatings, polymer coatings and bioglass coatings [61]. Using these coatings to protect the BMG against initial

Table 2
Characteristics of bioceramics and bulk metallic glasses.

Material	Young's modulus (GPa)	Compressive strength (MPa)	Density (g cm^{-3})	Degradation in vivo	References
HA	73–117	~600	~3.1	~1–2% per year	[46,49,52,57]
Bioglass	~30–75	~500–1000	~2.5	Bioactive	[6,52]
TCP	~70–90	~400–700	~2.9	15 weeks	[46,52,58,59]
$CaSO_4$				~6–8 weeks	[49,52]
MgZnCa BMG	~41–45	~675–894	1.74–2.0		[21,23]
CaMgZn BMG	~17–22.3	~300–608	~2.0	~4 weeks	[30]
Cortical bone	~3–30	~130–180	~1.6–2.1	Human bone remodeling time ~20–25 weeks	[46,49,52]

degradation, CaMgZn BMG could serve as mechanical supports for potential orthopedic applications, and after healing of the damaged bone it would be then absorbed without requiring a second operation for to removing remove the implant. In future studies the degradation rate of the CaMgZn BMG alone should not be regarded as the only factor determining mechanical stability when implanted in vivo, with degradation-induced bone formation around the rod needing to be included. Thus the mechanical properties of the bone–CaMgZn BMG complex should be tested together to understand the real clinical impact.

5. Conclusions

In brief, CaMgZn BMG may be a promising biodegradable biomaterial and a suitable bone substituent, based on the following conclusions.

1. CaMgZn BMG is biodegradable in Hank's solution, with a degradation time as fast as three hours, while there is little BMG sample left 4 weeks after implantation in the mouse marrow cavity because of the confined area.
2. CaMgZn BMG extracts show good biocompatibility over a wide range of concentrations. It does not result in the cell death of L929, VSMC, and ECV304 cells over a wide range of concentrations. It can promote the viability of MG63 cells as well as ALP production in the concentration range ~10–30%, which may benefit new bone formation.
3. Although higher concentrations can cause apoptosis of MG63 cells and also change the cell morphology, MG63 cells incubated with CaMgZn BMG extracts at low concentrations have a well stretched F-actin distribution and clear nuclei.
4. When implanted into bone low density CaMgZn BMG was degraded in vivo and the debris could stimulate new bone formation. There was no inflammation observed and no mice died. So, with a Young's modulus close to that of human bone, CaMgZn BMG might accelerate symphysis in bone defects, which suggests their potential application in orthopedics, as absorbable screws or plates, especially for osteoporotic fracture fixation and repair. However, certain regions showing osteolysis induced by rapid degradation of the materials imply the need for further material improvement or surface modification.

Acknowledgements

This work was supported by the Research Fund for the Doctoral Program of Higher Education under Grant No. 20100001110011, National High Technology Research and Development Program of China (863 Program) under Grant No. 2011AA030101 and 2011AA030103, the National Natural Science Foundation of China (No. 30770580) and the Program for New Century Excellent Talents in University (NCET-07-0033).

Appendix A. Figures with essential colour discrimination

Certain figures in this article, particularly Figures 1, 2, 4, 8, 10 and 12–15, are difficult to interpret in black and white. The full colour images can be found in the on-line version, at doi:10.1016/j.actbio.2011.04.027.

Appendix B. Supplementary data

Supplementary data associated with this article can be found, in the online version, at doi:10.1016/j.actbio.2011.04.027.

References

[1] Wang M. Developing bioactive composite materials for tissue replacement. Biomaterials 2003;24:2133.
[2] Salman SM, Salama SN, Darwish H, Abo-Mosallam HA. In vitro bioactivity of glass-ceramics of the $CaMgSi_2O_6$–$CaSiO_3$–Ca-5(PO_4)(3)F–Na_2SiO_3 system with TiO_2 or ZnO additives. Ceram Int 2009;35:1083.
[3] Cai S, Zhang WJ, Xu GH, Li JY, Wang DM, Jiang W. Microstructural characteristics and crystallization of CaO–P_2O_5–Na_2O–ZnO glass ceramics prepared by sol–gel method. J Non-Cryst Solids 2009;355:273.
[4] Wong A, Howes AP, Dupree R, Smith ME. Natural abundance Ca-43 NMR study of calcium-containing organic solids: a model study for Ca-binding biomaterials. Chem Phys Lett 2006;427:201.
[5] Alam MI, Asahina I, Ohmamiuda K, Takahashi K, Yokota S, Enomoto S. Evaluation of ceramics composed of different hydroxyapatite to tricalcium phosphate ratios as carriers for rhBMP-2. Biomaterials 2001;22:1643.
[6] Vogel M, Voigt C, Gross UM, Muller-Mai CM. In vivo comparison of bioactive glass particles in rabbits. Biomaterials 2001;22:357.
[7] Burkhart SS. The evolution of clinical applications of biodegradable implants in arthroscopic surgery. Biomaterials 2000;21:2631.
[8] Demetriou MD, Wiest A, Hofmann DC, Johnson WL, Han B, Wolfson N, et al. Amorphous metals for hard-tissue prosthesis. Jom-Us 2010;62:83.
[9] Schroers J, Kumar G, Hodges TM, Chan S, Kyriakides TR. Bulk metallic glasses for biomedical applications. Jom-Us 2009;61:21.
[10] Bai L, Cui CX, Wang QZ, Bu SJ, Qi YM. Ti–Zr–Fe–Si system amorphous alloys with excellent biocompatibility. J Non-Cryst Solids 2008;354:3935.
[11] Morrison ML, Buchanan RA, Peker A, Liaw PK, Horton JA. Electrochemical behavior of a Ti-based bulk metallic glass. J Non-Cryst Solids 2007;353:2115.
[12] Liu L, Qiu CL, Sun M, Chen Q, Chan KC, Pang GKH. Improvements in the plasticity and biocompatibility of Zr–Cu–Ni–Al bulk metallic glass by the microalloying of Nb. Mater Sci Eng A Struct Mater Properties Microstruct Process 2007;449:193.
[13] Buzzi S, Jin KF, Uggowitzer PJ, Tosatti S, Gerber T, Loffler JF. Cytotoxicity of Zr-based bulk metallic glasses. Intermetallics 2006;14:729.
[14] Qiu CL, Liu L, Sun M, Zhang SM. The effect of Nb addition on mechanical properties, corrosion behavior, and metal-ion release of ZrAlCuNi bulk metallic glasses in artificial body fluid. J Biomed Mater Res Part A 2005;75A:950.
[15] Morrison ML, Buchanan RA, Leon RV, Liu CT, Green BA, Liaw PK, et al. The electrochemical evaluation of a Zr-based bulk metallic glass in a phosphate-buffered saline electrolyte. J Biomed Mater Res Part A 2005;74A:430.
[16] Qin FX, Wang XM, Xie GQ, Inoue A. Distinct plastic strain of Ni-free Ti–Zr–Cu–Pd–Nb bulk metallic glasses with potential for biomedical applications. Intermetallics 2008;16:1026.
[17] Wang YB, Li HF, Cheng Y, Wei SC, Zheng YF. Corrosion performances of a nickel-free Fe-based bulk metallic glass in simulated body fluids. Electrochem Commun 2009;11:2187.
[18] Oak JJ, Louzguine-Luzgin DV, Inoue A. Investigation of glass-forming ability, deformation and corrosion behavior of Ni-free Ti-based BMG alloys designed for application as dental implants. Mater Sci Eng C Biomimetic Supramol Syst 2009;29:322.
[19] Liu L, Qiu CL, Chen Q, Chan KC, Zhang SM. Deformation behavior, corrosion resistance, and cytotoxicity of Ni-free Zr-based bulk metallic glasses. J Biomed Mater Res Part A 2008;86A:160.
[20] Huang L, Cao Z, Meyer HM, Liaw PK, Garlea E, Dunlap JR, et al. Responses of bone-forming cells on pre-immersed Zr-based bulk metallic glasses: effects of composition and roughness. Acta Biomater 2011;7:395.
[21] Zberg B, Uggowitzer PJ, Loffler JF. MgZnCa glasses without clinically observable hydrogen evolution for biodegradable implants. Nat Mater 2009;8:887.
[22] Zberg B, Arata ER, Uggowitzer PJ, Loffler JF. Tensile properties of glassy MgZnCa wires and reliability analysis using Weibull statistics. Acta Mater 2009;57:3223.
[23] Gu XN, Zheng YF, Zhong SP, Xi TF, Wang JQ, Wang WH. Corrosion of, and cellular responses to Mg–Zn–Ca bulk metallic glasses. Biomaterials 2010;31:1093.
[24] Ma E, Xu J. Biodegradable alloys. The glass window of opportunities. Nat Mater 2009;8:855.
[25] Zhao YY, Ma E, Xu J. Reliability of compressive fracture strength of Mg–Zn–Ca bulk metallic glasses: flaw sensitivity and Weibull statistics. Scripta Mater 2008;58:496.
[26] Park ES, Kim DH. Formation of Ca–Mg–Zn bulk glassy alloy by casting into cone-shaped copper mold. J Mater Res 2004;19:685.
[27] Park ES, Kim DH. Design of bulk metallic glasses with high glass forming ability and enhancement of plasticity in metallic glass matrix composites: a review. Met Mater Int 2005;11:19.
[28] Senkov ON, Miracle DB, Keppens V, Liaw PK. Development and characterization of low-density Ca-based bulk metallic glasses: an overview. Metall Mater Trans A 2008;39A:1888.
[29] Morrison ML, Buchanan RA, Senkov ON, Miracle DB, Liaw PK. Electrochemical behavior of Ca-based bulk metallic glasses. Metall Mater Trans A 2006;37A:1239.
[30] Wang G, Liaw PK, Senkov ON, Miracle DB, Morrison ML. Mechanical and fatigue behavior of Ca65Mg15Zn20 bulk-metallic glass. Adv Eng Mater 2009;11:27.
[31] Amiya K, Inoue A. Formation and thermal stability of Ca–Mg–Ag–Cu bulk glassy alloys. Mater Trans 2002;43:2578.

[32] Amiya K, Inoue A. Formation, thermal stability and mechanical properties of Ca-based bulk glassy alloys. Mater Trans 2002;43:81.
[33] Ilich JZ, Kerstetter JE. Nutrition in bone health revisited: a story beyond calcium. J Am Coll Nutr 2000;19:715.
[34] Serre CM, Papillard M, Chavassieux P, Voegel JC, Boivin G. Influence of magnesium substitution on a collagen–apatite biomaterial on the production of a calcifying matrix by human osteoblasts. J Biomed Mater Res 1998;42:626.
[35] Li ZJ, Gu XN, Lou SQ, Zheng YF. The development of binary Mg–Ca alloys for use as biodegradable materials within bone. Biomaterials 2008;29:1329.
[36] Towler MR, Boyd D, Freeman C, Brook IM, Farthing P. Comparison of in vitro and in vivo bioactivity of SrO–CaO–ZnO–SiO_2 glass grafts. J Biomater Appl 2009;23:561.
[37] Yamaguchi M. Role of zinc in bone formation and bone resorption. J Trace Elem Exp Med 1998;11:119.
[38] Yamaguchi M, Oishi H, Suketa Y. Stimulatory effect of zinc on bone-formation in tissue-culture. Biochem Pharmacol 1987;36:4007.
[39] Hanzi AC, Gerber I, Schinhammer M, Loffler JF, Uggowitzer PJ. On the in vitro and in vivo degradation performance and biological response of new biodegradable Mg–Y–Zn alloys. Acta Biomater 2010;6:1824.
[40] Siu WS, Qin L, Cheung WH, Leung KS. A study of trabecular bones in ovariectomized goats with micro-computed tomography and peripheral quantitative computed tomography. Bone 2004;35:21.
[41] Nayab SN, Jones FH, Olsen I. Effects of calcium ion implantation on human bone cell interaction with titanium. Biomaterials 2005;26:4717.
[42] Barnard BR, Liaw PK, Buchanan RA, Senkov ON, Miracle DB. Oxidation behavior of Ca-based bulk amorphous materials. Mater Trans 2007;48:1870.
[43] Jinno T, Kirk SK, Morita S, Goldberg VM. Effects of calcium ion implantation on osseointegration of surface-blasted titanium alloy femoral implants in a canine total hip arthroplasty model. J Arthroplasty 2004;19:102.
[44] Hanawa T. In vivo metallic biomaterials and surface modification. Mat Sci Eng A Struct 1999;267:260.
[45] Chen KY, Shyu PC, Dong GC, Chen YS, Kuo WW, Yao CH. Reconstruction of calvarial defect using a tricalcium phosphate–oligomeric proanthocyanidins cross-linked gelatin composite. Biomaterials 2009;30:1682.
[46] Hamadouche M, Sedel L. Ceramics in orthopaedics. J Bone Joint Surg Br 2000;82B:1095.
[47] Suchanek W, Yashima M, Kakihana M, Yoshimura M. Processing and mechanical properties of hydroxyapatite reinforced with hydroxyapatite whiskers. Biomaterials 1996;17:1715.
[48] Fu L, Khor KA, Lim JP. Processing, microstructure and mechanical properties of yttria stabilized zirconia reinforced hydroxyapatite coatings. Mat Sci Eng A Struct 2001;316:46.
[49] Cao WP, Hench LL. Bioactive materials. Ceram Int 1996;22:493.
[50] Akao M, Aoki H, Kato K, Sato A. Dense polycrystalline beta-tricalcium phosphate for prosthetic applications. J Mater Sci 1982;17:343.
[51] Zyman ZZ, Tkachenko MV, Polevodin DV. Preparation and characterization of biphasic calcium phosphate ceramics of desired composition. J Mater Sci Mater Med 2008;19:2819.
[52] Hench LL. Bioceramics – from concept to clinic. J Am Ceram Soc 1991;74:1487.
[53] Lang NP, Bragger U, Hammerle C, Sutter F. Immediate transmucosal implants using the principle of guided tissue regeneration. 1. Rationale, clinical procedures and 30-month results. Clin Oral Implan Res 1994;5:154.
[54] Bragger U, Hammerle CHF, Lang NP. Immediate transmucosal implants using the principle of guided tissue regeneration. 2. A cross-sectional study comparing the clinical outcome 1 year after immediate to standard implant placement. Clin Oral Implant Res 1996;7:268.
[55] Yeo A, Rai B, Sju E, Cheong JJ, Teoh SH. The degradation profile of novel, bioresorbable PCL-TCP scaffolds: an in vitro and in vivo study. J Biomed Mater Res A 2008;84A:208.
[56] MacKenzie KJD, Rahner N, Smith ME, Wong A. Calcium-containing inorganic polymers as potential bioactive materials. J Mater Sci 2010;45:999.
[57] Fulmer MT, Ison IC, Hankermayer CR, Constantz BR, Ross J. Measurements of the solubilities and dissolution rates of several hydroxyapatites. Biomaterials 2002;23:751.
[58] Li YB, Kong FZ, Weng WJ. Preparation and characterization of novel biphasic calcium phosphate powders (alpha-TCP/HA) derived from carbonated amorphous calcium phosphates. J Biomed Mater Res B 2009;89B:508.
[59] Chen BQ, Zhang ZQ, Zhang JX, Lin QL, Jiang DL. Fabrication and mechanical properties of beta-TCP pieces by gel-casting method. Mat Sci Eng C Bio S 2008;28:1052.
[60] Li HF, Wang YB, Cheng Y, Zheng YF. Surface modification of Ca60Mg15Zn25 bulk metallic glass for slowing down its biodegradation rate in water solution. Mater Lett 2010;64:1462.
[61] Skipper LJ, Sowrey FE, Pickup DM, Fitzgerald V, Rashid R, Drake KO, et al. Structural studies of bioactivity in sol–gel-derived glasses by X-ray spectroscopy. J Biomed Mater Res A 2004;70A:354.